Electrochemical characterization of hydroquinone derivatives with different substituent in acetonitrile

ARTICLE *in* NEW JOURNAL OF CHEMISTRY · FEBRUARY 2015

Impact Factor: 3.16 · DOI: 10.1039/C4NJ01657B

5 AUTHORS, INCLUDING:

Ricardo Salazar
University of Santiago, Chile
28 PUBLICATIONS **140** CITATIONS
SEE PROFILE

Maximiliano Martínez-Cifuentes
Universidad de Talca
11 PUBLICATIONS **5** CITATIONS
SEE PROFILE

Ramiro Araya-Maturana
University of Chile
95 PUBLICATIONS **269** CITATIONS
SEE PROFILE

Oney Ramírez-Rodríguez
University of Chile
10 PUBLICATIONS **17** CITATIONS
SEE PROFILE

NJC

PAPER

Cite this: *New J. Chem.*, 2015, **39**, 1237

Electrochemical characterization of hydroquinone derivatives with different substituents in acetonitrile

Ricardo Salazar,*[a] Jorge Vidal,[a] Maximiliano Martínez-Cifuentes,[b] Ramiro Araya-Maturana[c] and Oney Ramírez-Rodríguez*[c]

Received (in Porto Alegre, Brazil) 26th September 2014,
Accepted 25th November 2014

DOI: 10.1039/c4nj01657b

www.rsc.org/njc

The effect of carbonyl groups in the *ortho* position with respect to a hydroxyl group on the electrochemical oxidation of hydroquinones in acetonitrile is studied. The electrochemical response of hydroquinone on a glassy carbon electrode in 0.1 M tetrabutylammonium perchlorate was investigated in detail by voltammetry and coulometry. From these experiments, the oxidation potential was shifted to more positive values with respect to hydroquinone due to the presence of electron withdrawing groups bonded to the aromatic ring. For all compounds a diffusional behavior was observed, and the diffusion coefficient (*D*) of substituted hydroquinones was calculated showing higher values than found for unsubstituted hydroquinone. Theoretical calculations were carried out to gain insights into the intramolecular hydrogen bond present in these molecules affecting their electrochemical behavior. Relevant theoretical data are optimized geometrical parameters, HOMO energy, condensed radical Fukui functions (f°), natural charges, Wiberg bond orders (WBO), stabilization energies caused by electron transfer, and hyperconjugation stabilization energies from the NBO analysis. In most cases, the calculations show good agreement with experimental ^{1}H-NMR data and support the electrochemical results.

1. Introduction

The *o*- and *p*-dihydroxybenzene moieties are widely distributed in nature. They are oxidized, generally under mild conditions, to yield quinones. Cells use this type of reaction to transport an electron pair from one substance to another, for example, in mitochondrial ATP synthesis and in photosynthesis.[1,2] For this reason, the study of the electron and proton transfer mechanism of the *p*-quinone/*p*-hydroquinone and *o*-quinone/catechol systems is a matter of great theoretical[3–5] and experimental interest.[6–11]

Furthermore, the dihydroxybenzene isomers are widely used in many fields, such as cosmetics, dyes, and pharmaceutical and chemical industries. Quinones, hydroquinones, catechols and resorcinols have biological properties that include anti-tumor,[12–14] antimicrobial[15,16] and antifungal activity,[17,18] among others.[19–21]

Many studies in aprotic and protic media have shown the effect of Brønsted bases and acids on the electrochemistry of quinoid compounds by hydrogen bond formation and proton transfer.[22–24] The oxidation of H-bonded phenols generally takes place by concerted proton–electron transfer (CPET) reactions,[25–28] although there are some exceptions.[29,30] The importance of proton transfer is also indicated by the substantially larger rate constants for compounds which can undergo proton loss *vs.* compounds which cannot undergo proton loss with the same photo-oxidant.[31]

A correlation between ^{1}H-NMR chemical shift and IR frequency as indicators of H-bond strength, and the quinone half-wave reduction potential has been described, showing that the strong hydrogen bonds make the reduction of quinones easier.[32] Many other authors have published results of hydroquinones oxidation or quinone reduction having intramolecular hydrogen bonds. In all cases it has been shown that the formation of intramolecular hydrogen bonds causes a substantial variation of the half-wave potential.[31–34]

The electro-oxidation of phenols and derivatives has a very complex mechanism, as shown in Scheme 1. There are many species related by electron and proton transfer which occurs as a consequence of bimolecular interactions and primary electrode processes. The experimental variables have proven to be crucial in the predominance of one species over another.[35]

The possible products formed from the phenoxonium ion (**IV**) (Scheme 2) can be divided into two groups, depending on the reaction pathway. If the substituent is OH, *ortho*- or

[a] *Department of Environmental Sciences, Faculty of Chemistry and Biology, University of Santiago de Chile, USACh, Casilla 40, Correo 33, Santiago, Chile. E-mail: ricardo.salazar@usach.cl; Tel: +56-2-2718-1134*

[b] *Laboratory of Asymmetric Synthesis, Chemistry Institute of Natural Resources, University of Talca, Casilla 747, Talca, Chile*

[c] *Department of Organic and Physical Chemistry, Faculty of Chemical and Pharmaceutical Sciences, University of Chile, Casilla 233, Santiago 1, Chile. E-mail: oramirez@ciq.uchile.cl; Tel: +56-2-2978-2900*

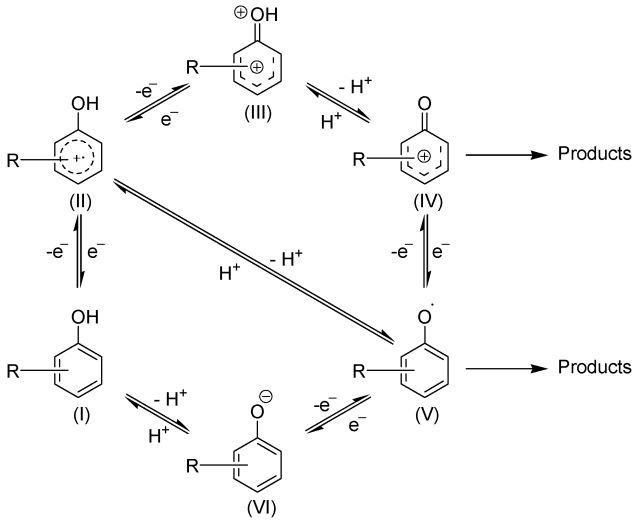

Scheme 1 Electro-oxidation of phenol and derivatives.

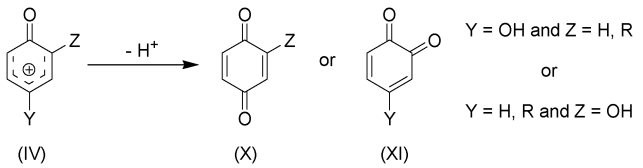

Scheme 2 Quinones formed by proton loss from the phenoxonium ion.

para-benzoquinone derivatives (**X** and **XI**) are formed by proton loss from the *ortho*- or *para*-hydroxyl group on the phenoxonium ion (**IV**).[35]

Electrochemical studies using cyclic voltammetry, chronoamperometry, chronocoulometry, differential pulse voltammetry, linear sweep voltammetry, *etc.*, have been used to investigate mechanistic, kinetic and electroanalytical aspects of the quinone/hydroquinone redox system.[36–39] On the other hand, several theoretical calculation methods are used to study molecules and their reactions. The natural bond orbital (NBO) method[40] has been recognized as a powerful tool to get insights into orbital interactions, stabilization energies caused by electron transfer, and hyperconjugation stabilization energies.[41,42] The NBOs are one of the consequences of natural localized orbital sets that include natural atomic (NAO), hybrid (NHO) and semi-localized molecular orbital (NLMO) sets, intermediate between basis atomic orbitals (AOs) and canonical molecular orbitals (MOs).[40]

$$\text{AOs} \rightarrow \text{NAOs} \rightarrow \text{NHOs} \rightarrow \text{NBOs} \rightarrow \text{NLMOs} \rightarrow \text{MOs} \quad (1)$$

The NBO method involves population analysis, which distributes computed electron density to orbitals in the way a chemist thinks in terms of physical organic chemistry. The interaction between bonding and antibonding orbitals represents the deviation of the molecule from the Lewis structure and can be used as a measure of the delocalization due to the presence of hydrogen bonding interaction.[40] The hyperconjugative interaction between lone pair (LP) on acceptor oxygen and sigma antibonding on donor H–O (LPO → σ*H–O′) in the O···H–O′ complex has been described as a major contribution to hydrogen bond interaction obtained by NBO analysis.[43–45] With second-order perturbation theory analysis, the donor–acceptor interaction (stabilization energy) can be calculated.[40]

In this paper we study the effect of carbonyl groups in the *ortho* position with respect to a hydroxyl group on the electrochemical oxidation of hydroquinones in acetonitrile. The electrochemical response of hydroquinone on a glassy carbon electrode in 0.1 M tetrabutylammonium perchlorate was investigated in detail by voltammetry and coulometry. From these experiments, we determined the influence of the substituent on the electrochemical oxidation peak, the transferred electron numbers, the diffusional process and diffusion coefficient (D) of hydroquinones. The oxidation potentials were correlated with theoretical parameters.

2. Experimental

2.1. Hydroquinones

Hydroquinone (**HQ**), 2′,5′-dihydroxyacetophenone (**HQ1**), 2,5-dihydroxybenzoic acid (**HQ2**), 2′,4′-dihydroxyacetophenone (**HQ6**) and 3,4-dihydroxybenzoic acid (**HQ8**) are commercially available and were used without further purification. Ethyl 2,5-dihydroxybenzoate (**HQ3**) was synthesized by Fischer esterification, using **HQ2** and ethanol as reagents and sulfuric acid as a catalyst; their physical constants agree with those reported in the literature.[46] 2-Bromo-1-(2,5-dihydroxyphenyl)ethanone (**HQ4**) and 1-(2-chloro-3,6-dihydroxyphenyl)ethanone (**HQ7**) were synthesized by described procedures.[47,48] The chemical structures of all the studied hydroquinones are shown in Fig. 1.

Synthesized compounds. 1-(2,5-Dihydroxyphenyl)-2-iodoethanone (**HQ5**)

Four hundred milligrams (1.73 mmol) of 2-bromo-1-(2,5-dihydroxyphenyl)ethanone (**HQ4**) were dissolved in 50 mL of acetone and then 649 mg (4.3 mmol) of sodium iodide dissolved in 20 mL of acetone was added. The reaction mixture was stirred for 2 hours and was then heated under reflux for 30 minutes. The solvent was removed under vacuum and the residue was purified by flash column chromatography on silica gel using a 2 : 1 mixture of hexane–ethyl acetate.

Yellow solid. Yield: 80%. MP: 120.5–121 °C. IR (KBr, cm^{-1}) 3287, 3221, 3179, 1642, 1618, 1569, 1484, 1476, 1425, 1367, 1309, 1263, 1209, 1086, 1011, 924, 833, 829, 789, 647. ^{1}H-NMR ($CDCl_3$, 300 MHz) δH 4.32 (s, 2H, CH_2), 4.75 (s, 1H, HO–C5), 6.93 (d, J = 8.9 Hz, 1H, H–C3), 7.08 (dd, J = 2.9, 8.9 Hz, 1H, H–C4), 7.18 (d, J = 2.9 Hz, 1H, H–C6), 11.46 (s, 1H, HO–C2). ^{13}C-NMR (75 MHz, DMSO-d_6) δC 6.75, 115.32, 118.54, 118.64, 124.49, 149.51, 153.21, 197.27. HRMS (EI, 70 eV) M^+ m/z 277.94423 – calculated for $C_8H_7IO_3$: 277.94399.

2.2. Electrochemical experiments

2.2.1. Electrolytic medium: acetonitrile containing 0.1 M tetrabutylammonium perchlorate (TBAP). The working concentrations of each hydroquinone varied between 0.1 mM and 2 mM.

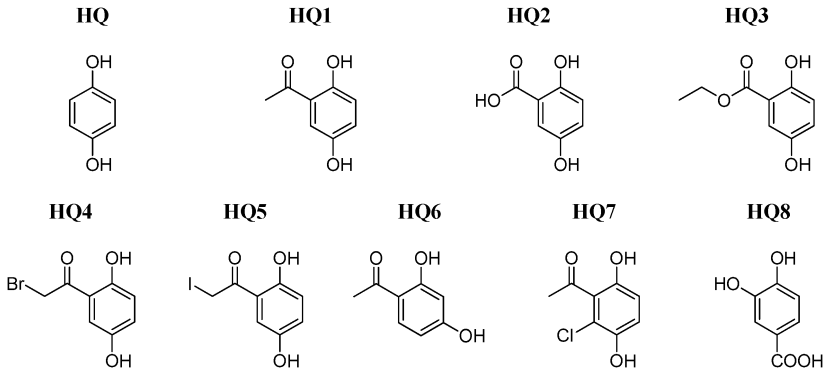

Fig. 1 Chemical structures of the investigated compounds.

2.2.2. Differential pulse voltammetry (dpv), cyclic voltammetry (cv) and linear sweep voltammetry (lsv). They were carried out with a CH Instrument 760-C electrochemical work station. All the voltammetric experiments were carried out with 1.0 mM solutions of each hydroquinone. A stationary glassy carbon electrode (GCE, CH Instrument, with an area of 0.0707 cm^2) was used as a working electrode for the dpv and cv experiments. For hydrodynamic experiments, a rotating disk glassy carbon electrode was employed (CH Instrument, with an area of 0.0707 cm^2). The surface of the disk was polished to a mirror finish with 0.1 μm alumina powder before use and after each measurement. Platinum wire was used as an auxiliary electrode, and all potentials were measured against a nonaqueous Ag/Ag^+ reference electrode CH Instrument 112. For all experiments, the resistance was compensated automatically.

2.2.3. Coulometric analyses. Studies on exhaustive electrolysis were carried out for two hours at constant electrode potential (+0.2 V peak potential found by dpv showed in Table 1) in a divided cell, on a glassy carbon mesh electrode using 30 mL of 1×10^{-5} M solutions of the compounds. A three-electrode circuit with a reference non aqueous Ag/Ag^+ and platinum wire as a counter electrode were used. A CH Instrument 760-C assembly was used to electrolyze the hydroquinone solutions. The net charge was calculated, including correction for the estimated background current.

Table 1 Kinetic and electrochemical parameters of hydroquinone and its derivatives

Derivative	E_p [a]/V	n [b]	ΔE_p [c]/V	D/cm^2 s^{-1}
HQ	0.880	2.023	0.553	2.77×10^{-5}
HQ1	1.028	1.986	0.798	2.61×10^{-5}
HQ2	1.024	1.883	0.458	2.60×10^{-5}
HQ3	1.032	1.857	0.721	2.40×10^{-5}
HQ4	1.080	1.789	0.639	2.06×10^{-5}
HQ5	1.076	1.792	0.692	1.82×10^{-5}
HQ6	1.632	1.655	0.832	2.16×10^{-5}
HQ7	0.920	2.136	0.717	2.16×10^{-5}
HQ8	1.064	1.955	0.519	2.58×10^{-5}

[a] Oxidation potential obtained (*vs.* Ag/AgCl sat) from dpv experiments of 1.0 mM solutions in acetonitrile + 0.1 M tetrabutylammonium perchlorate. [b] Electron numbers obtained by coulometric experiments of 1.0×10^{-5} M solutions of **HQ** and **HQ** derivatives in acetonitrile + 0.1 M tetrabutylammonium perchlorate. The assays were made three times (RSD = ±0.0426). [c] $\Delta E_p = E_{pa} - E_{pc}$ for cv experiments at 0.1 V s^{-1}.

2.2.4. Characterization of the synthesized compounds. Melting points were uncorrected and measured on a Büchi SMP-20 or a Gallenkamp melting point apparatus. Infrared spectra were recorded on a NICOLET 510P FT-IR spectrophotometer for KBr discs, and the frequencies are given in cm^{-1}. NMR spectra were obtained on a Bruker AVANCE DRX 300 instrument at 300.13 and 75.5 MHz for ^1H and ^{13}C NMR, respectively. Chemical shifts (δ) are reported in parts per million downfield from TMS for ^1H NMR, or relative to residual solvent signals ($CHCl_3$, 7.26 ppm for ^1H NMR, DMSO-d_6, 39.52 ppm for ^{13}C NMR spectra). ^{13}C NMR spectra were acquired on a broad-band decoupled mode. Silica gel 60 (230–400 mesh ASTM) and DC-Alufolien 60 F_{254} were used for flash-column chromatography and analytical TLC, respectively.

2.2.5. Theoretical calculations. The calculations were carried out using the Gaussian 03 program package.[49] Geometries were optimized at the B3LYP/6-311++G** level for C, H, O, Cl, and Br, and at the B3LYP/SDB-cc-pVTZ level for I. No imaginary frequencies were found at the optimized molecular geometries, indicating that they are real minima of the potential energy surface. NBO calculation was carried out with the 6-311G** basis set to avoid the problems associated with diffuse functions in this kind of calculation.[50]

3. Results and discussion

3.1. Differential pulse voltammetry (dpv) results

Dpv results reveal that **HQ** and **HQ** derivatives exhibited one well-defined anodic peak at potentials higher than +0.8 V *versus* $Ag/AgCl_{(sat)}$ (Fig. 2 and Table 1). Oxidation peak potential values of **HQ** derivatives were shifted towards more positive values compared with **HQ** ($E_{p,\mathbf{HQ}}$ = +0.88 V). The results of the oxidations of **HQ** and **HQ** derivatives are shown in Fig. 2 and Table 1.

Oxidation of these hydroquinones is dependent on two factors: the electronic effects of substituents on the aromatic ring, and the formation of an intramolecular hydrogen bond (IHB) between a hydroxyl group and a substituent in the *ortho*-position (Fig. 1). The oxidation potential of the substituted HQs is increased compared to **HQ** due to the presence of electron withdrawing groups bonded to the aromatic ring, because they decrease its electron density as well as that on the hydroxyl

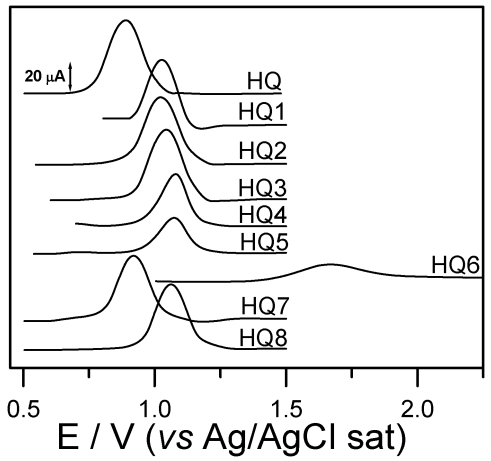

Fig. 2 D_p voltammograms of 1.0 mM solutions of the investigated compounds. Non aqueous medium: acetonitrile + 0.1 M tetrabutylammonium perchlorate.

oxygen atom, hindering the loss of one electron from it. Additionally, the potential depends on the strength of the intramolecular hydrogen bond of the phenolic hydroxyl. A strong hydrogen bond facilitates oxidation because it increases the electron density on the oxygen atom, facilitating the transfer of electrons.

To explore and quantify both the effects of a substituent on the ring and the IHB, and establish their relationship with the oxidation potential we used DFT calculations (Table 2).

3.2. DFT calculations

The optimized geometric parameters, HOMO energy and condensed radical Fukui functions (f°) are summarized in Table 3, respectively. The natural charges (q) and the Wiberg bond order (WBO) from the NBO analysis for the optimized geometries from **HQ** to **HQ8** are presented in Tables 4 and 5, respectively. The stabilization energies for selected NBO donor–acceptor pairs in the HQs, given by second order perturbation energies of the Fock matrix in the NBO basis, are presented in Table 6. According to these results, substituents on the aromatic ring, for **HQ1** to **HQ8**, increase the O1–H1 distance compared to **HQ**. The differences in the O3···H1 distances and in the O1–H1–O3 angles between HQs (Table 3) are indicative of differences in the IHB strength. On the other hand, the condensed radical Fukui function indicates the most susceptible site for a radical attack leading to a loss or a gain of an electron. With this criterion we found that, for all HQs, O1 is the more reactive center for electron abstraction. Besides, the reduction of the natural charge on O1 should increase their oxidation potential compared to **HQ**. Our results show that **HQ1** to **HQ7** show a reduced natural charge on O1 compared with **HQ**, in agreement with the experimental data. On the other hand, the WBO reflect the change caused by aromatic ring substituents on the intramolecular hydrogen bond, which also affects the ability of the HQs to transfer electrons. The WBO for O3···H1 changes from **HQ1** to **HQ7** depending on the nature of the carbonyl group and the aromatic ring substituents.

Compounds **HQ1–3** show a similar E_p (range ±8 mV), and these three molecules show an electron-withdrawing group (acetyl, carboxyl and ethoxycarbonyl, respectively) in the *ortho*-position with respect to a phenol function (Fig. 1). The presence of these groups causes a decrease of the electron density on O1, as reflected in their natural charge for **HQ1–3** compared with **HQ**, and hence making them more difficult to oxidize. The oxidation potential is shifted about 140–150 mV higher than that of **HQ**.

The IHB O1–H1···O3 with acetyl in **HQ1** is stronger than with carboxyl in **HQ2** and with ethoxycarbonyl in **HQ3**, as reflected in the shorter distance and higher WBO for O3···H1 in **HQ1** compared to **HQ2** and **HQ3**. The latter is also reflected by hyperconjugative interaction between LPs of O3 and σ* of O1–H1, with the stabilization energy higher for **HQ1** (22.53 kcal mol^{-1}) compared to **HQ2** (15.78 kcal mol^{-1}) and **HQ3** (16.73 kcal mol^{-1}), indicating a strong IHB for the first case. These results are consistent with a higher ^{1}H-NMR chemical shift for H1 in **HQ1** (δ_{H1} 11.81 ppm) compared with **HQ3** (δ_{H1} 10.48 ppm), and this greater deshielding of H1 in **HQ1** also reveals a strong IHB. For this reason, taking into account the IHB strength, **HQ1** should be oxidized more easily. However, it is possible also to argue that the greater strength of the hydrogen bond of the keto group, which facilitates oxidation, is counteracted by its greater electron-withdrawing effect, which hinders the transfer of electrons from the hydroxyl oxygen atom. The latter is supported by a higher stabilization energy for the LPs of O1 and σ* and π* for C1–Cα, which indicate the degree of delocalization of O1 on the aromatic ring. For **HQ1** LP of O1 and σ* and π* for C1–Cα interact with a stabilization energy of 43.59 kcal mol^{-1}, while for **HQ2** and **HQ3** the stabilization energies are 42.72 and 42.08 kcal mol^{-1}. The presence of these opposite operating effects explains the very similar potential of the three compounds.

On the other hand, **HQ4** and **HQ5** have an acetyl group the same as **HQ1**, but additionally, they possess a halogen atom in an α-position to the carbonyl group. **HQ4** has a bromine atom and **HQ5** an iodine atom instead (Fig. 1). They show a difference of approximately 50 mV with respect to **HQ1** (Table 1). A plausible explanation takes into account the differential electron withdrawing effect of the halogen atoms, due to their different electronegativities, on the carbonyl group. A higher electron density on the carbonyl group causes a strengthening of the IHB. The latter is reflected by the differences in the distance and WBO of O3···H1, because in **HQ1** $d_{O3\cdots H1}$ is 1.696 Å and WBO is 0.076, while in **HQ4** and **HQ5** $d_{O3\cdots H1}$ it increases to 1.711 Å and 1.707 Å, and the WBO is reduced to 0.072 and 0.070, respectively, all of which indicates a weakening of the IHB in **HQ4** and **HQ5**. Accordingly, hyperconjugative interaction between LPs for O3 and σ* for O1–H1 indicates a weaker IHB for **HQ4** and **HQ5** compared with **HQ1**. The chemical shift of H1 is 11.81 ppm for **HQ1**, 11.35 ppm for **HQ4** and 11.46 ppm for **HQ5**, showing the weakening of the IHB, in agreement with the theoretical parameters. Fig. 3 shows a good correlation between the chemical shift for chelated hydrogen (H1) and the Wiberg bond order (WBO) O3···H1. Moreover, the electron-withdrawing effect of α-haloacetyl groups is greater than that of the acetyl group, which is reflected by an increase of the stabilization energy for delocalization of O1 into C1–Cα,

Table 2 The optimized structures, HOMO and LUMO orbitals of the investigated HQs[a]

	Optimized structure	HOMO	LUMO
HQ	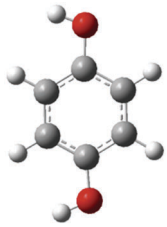	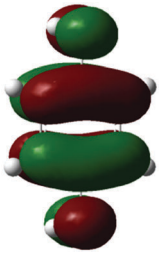	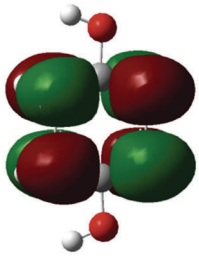
HQ1	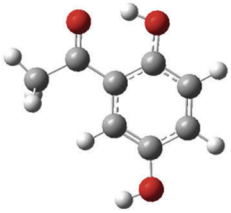	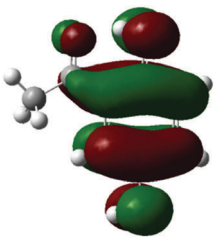	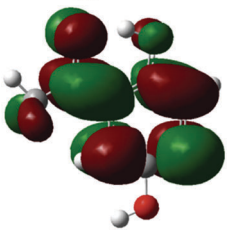
HQ2	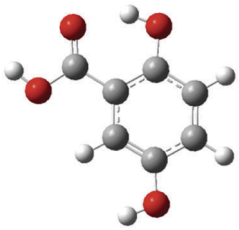	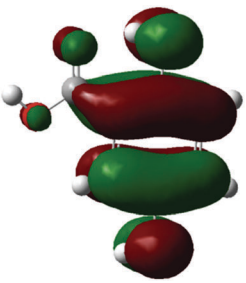	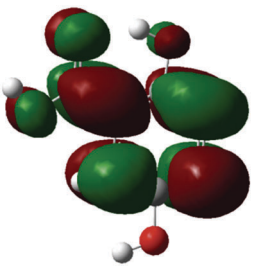
HQ3	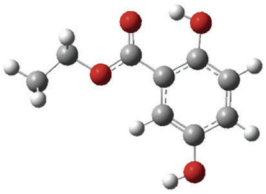	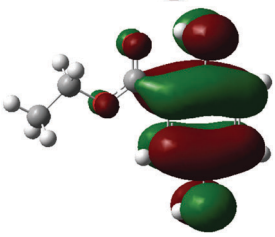	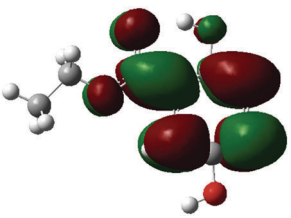
HQ4	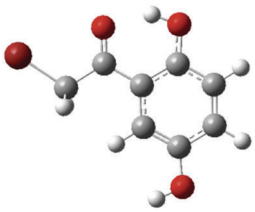	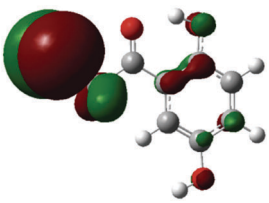	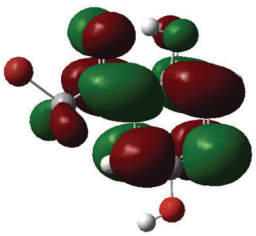
HQ5	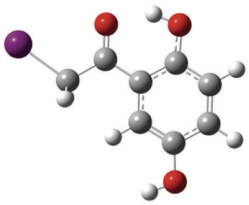	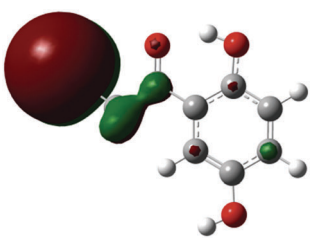	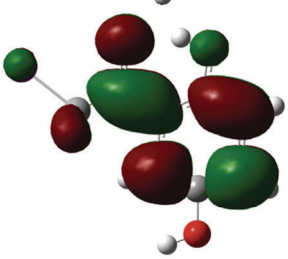
HQ6	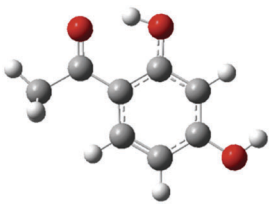	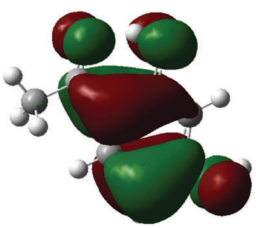	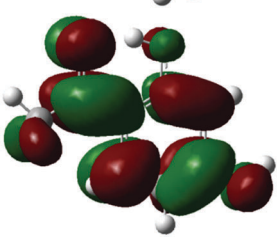

Table 2 (*continued*)

	Optimized structure	HOMO	LUMO
HQ7	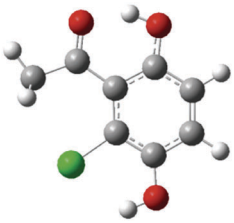	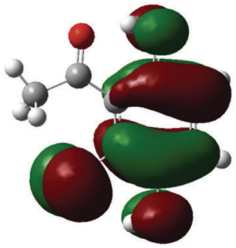	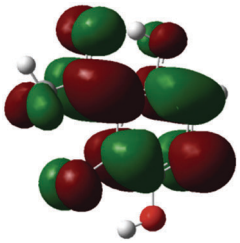
HQ8	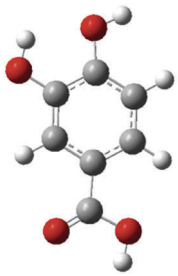	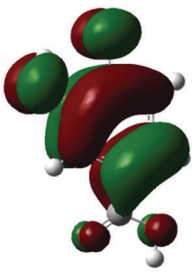	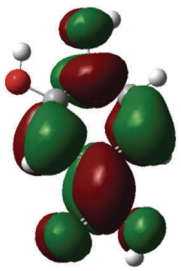

[a] B3LYP/6-311++G(d,p) is used for C, H, O, Cl and Br atoms. SDB-cc-pVTZ is used for I atom.

Table 3 Geometric parameters and condensed radical Fukui functions[a]

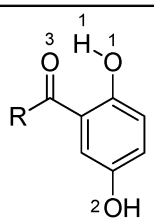

	$d_{O3\cdots H1}$	d_{O1-H1}	$\angle_{O1-H1-O3}$	E_{HOMO}	f°_{Ox1} (10^{-2})	f°_{Ox2} (10^{-2})	E_p (exp)
HQ	—	0.962	—	−0.21647	7.50	7.50	0.880
HQ1	1.696	0.986	146.310	−0.22618	9.18	6.96	1.028
HQ2	1.774	0.980	144.449	−0.22814	8.73	7.35	1.024
HQ3	1.760	0.981	145.066	−0.22206	8.84	7.18	1.032
HQ4	1.711	0.984	145.361	−0.23478	9.13	7.09	1.080
HQ5	1.707	0.984	145.397	−0.23378	9.13	7.10	1.076
HQ6	1.669	0.991	147.646	−0.24226	8.64	3.70	1.632
HQ7	1.591	0.993	147.341	−0.23160	9.16	6.87	0.920
HQ8	2.156	0.966	112.717	−0.23982	9.07	6.27	1.064

[a] Distances in Angström; angles in degrees, energies in a.u.; potentials (E_p) in volts; E in eV; f°_{Oxig} radical Fukui function.

from 31.87 kcal mol^{-1} for **HQ** to 44.46 kcal mol^{-1} and 44.42 kcal mol^{-1} for **HQ4** and **HQ5**, respectively. Therefore, the potential increases as a result of the decrease in the electron density of the aromatic ring. It is also reflected by an increase of the natural charge on O1.

The electronegative chlorine atom bonded in the *ortho*-position to the carbonyl group in **HQ7** reduces the natural charge on oxygen atom 1 and increases the WBO of O3···H1. Moreover, the electronic delocalization from chlorine to the acetyl group causes an increased hydrogen bond strength compared with **HQ1**, as is evidenced by the smaller stabilization energy of the LP of O3 interaction and σ* of O1–H1. All these factors explain why the oxidation potential of **HQ7** is 0.11 V lower than that of **HQ1**.

HQ1 and **HQ2** are isomers of **HQ6** and **HQ8**, respectively. **HQ1** and **HQ2** are *p*-hydroquinones, while **HQ6** is a resorcinol and **HQ8** is a catechol (*o*-hydroquinone). The IHB is stronger in **HQ6** compared to **HQ1**, according to the O3···H1 distance and the WBO. Stabilization energy for hyperconjugative interaction also indicates a strong IHB in **HQ6**. The strong electronic delocalization from the hydroxyl group located in the *para*-position

Table 4 Natural charges of the selected atoms in **HQ** compounds

	HQ	**HQ1**	**HQ2**	**HQ3**	**HQ4**	**HQ5**	**HQ6**	**HQ7**	**HQ8**
	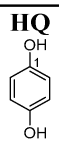	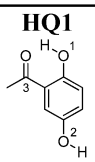	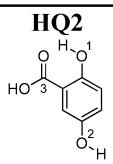	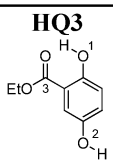	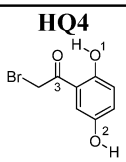	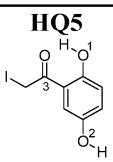	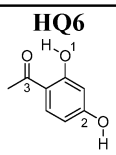	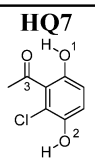	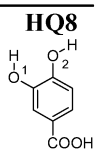
O1	−0.678	−0.672	−0.670	−0.673	−0.662	−0.663	−0.665	−0.661	−0.666
H1	0.459	0.502	0.494	0.493	0.494	0.494	0.493	0.491	0.477
O2		−0.677	−0.675	−0.677	−0.674	−0.674	−0.657	−0.672	−0.696
H2		0.466	0.462	0.461	0.462	0.462	0.467	0.474	0.477
O3		−0.611	−0.651	−0.654	−0.585	−0.591	−0.620	−0.609	

Table 5 Wiberg bond order for HQs

	HQ	HQ1	HQ2	HQ3	HQ4	HQ5	HQ6	HQ7	HQ8
C1–O1	0.998	1.101	1.086	1.083	1.098	1.103	1.115	1.116	1.026
O1–H1	0.775	0.658	0.679	0.676	0.671	0.662	0.654	0.641	0.752
C2–O2	0.998	1.007	1.009	1.006	1.003	1.010	1.035	1.024	0.995
O2–H2	0.775	0.768	0.766	0.768	0.772	0.767	0.767	0.743	0.757
C3–O3	—	1.656	1.628	1.613	1.666	1.674	1.627	1.632	—
O3···H1	—	0.076	0.054	0.057	0.072	0.070	0.090	0.105	—
Cl···H2	—	—	—	—	—	—	—	0.020	—
H1···O2	—	—	—	—	—	—	—	—	0.008

Table 6 Stabilization energies (kcal mol^{-1}) for select NBO pairs (donor–acceptor) given by second order perturbation energies of the Fock matrix in the NBO basis for the HQs

Donor	Type	Acceptor	Type	HQ	HQ1	HQ2	HQ3	HQ4	HQ5	HQ6	HQ7	HQ8
O1	LP (1)	C1–Cα	σ*	6.14	7.73	7.76	7.70	7.87	7.86	7.63	8.33	
O1	LP (2)	C1–Cα	π*	26.81	37.86	36.63	36.15	38.39	38.36	—	41.18	27.74
O2	LP (1)	C2–Cγ	σ*	—	6.32	6.31	6.24	6.41	6.40	6.23	7.26	6.18
O2	LP (2)	C2–Cγ	π*	—	27.33	27.23	26.89	27.95	27.87	31.63	31.49	26.01
O3	LP (1)	O1–H1	σ*	—	2.99	2.91	3.06	3.09	3.21	3.13	4.56	—
O3	LP (2)	O1–H1	σ*	—	19.31	12.78	13.68	17.26	17.46	22.27	28.77	—
Clγ	LP (2)	O2–H2	σ*	—	—	—	—	—	—	—	3.44	—
O1	LP (1)	C1–C2	σ*	—	—	—	—	—	—	—	—	6.54

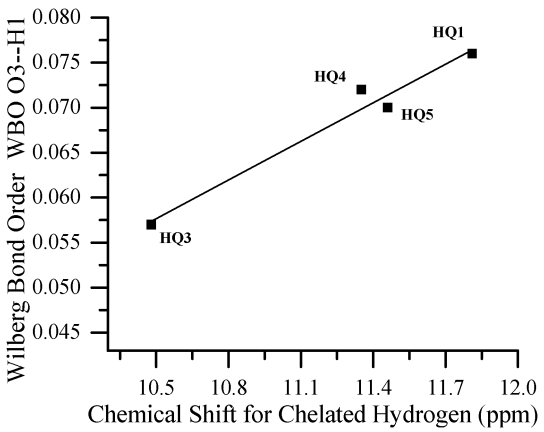

Fig. 3 Correlation between the chemical shift for chelated hydrogen (H1) and the Wiberg bond order (WBO) O3···H1.

relative to the acetyl group leads to a large increase in electron density of the carbonyl oxygen, thereby enhancing the hydrogen bond that facilitates oxidation. Despite the above, its reduction potential is greater than that of the other HQs. This can be explained by stabilization of semiquinone radicals from hydroquinones, which is not present in the radical derivate from resorcinols, as is the case of this molecule.

On the other hand, **HQ8** exhibits a weak IHB between H1···O2, with a distance of 2.156 Å and a WBO of 0.006. Non hyperconjugative stabilization energy was found for this interaction. Although **HQ8** has weaker IHB, it does not have a high reduction potential, which can be explained in terms of product stabilization. The *p*-quinones are more stable than the *o*-quinones because the carbonyl groups are further apart, thus the electron densities of the two carbon–oxygen π bonds do not affect each other; the carbonyl oxygen atoms, with a high electron density, are not close; and the carbonyl carbon atoms, electron deficient, are not neighbors. The greater stability of catechols compared to hydroquinones, and of *p*-quinones compared to *o*-quinones, determines that **HQ2** is oxidized more easily than **HQ8**. Zhu *et al.* report a comparison of hydride affinities between *o*-quinones and *p*-quinones, and demonstrate, using calculation methods, that *p*-benzoquinone is 5.5 kcal mol^{-1} more stable than *o*-benzoquinone, while the catechol monoanion is 7.3 kcal mol^{-1} more stable than the hydroquinone monoanion.[3]

3.3. Determination of transferred electrons by coulometric studies

As mentioned above, the oxidation reaction of hydroquinones and catechols in acetonitrile follows an electrochemical–chemical–electrochemical (ECE) sequence under a mixed kinetic control by electron and proton transfer. The determination of the electrons transferred during the oxidation of all HQs (Fig. 1), were based on the exhaustive electrolysis at controlled-potential using a three compartment cell. Glassy carbon mesh was used as a working electrode, a platinum wire as a counter electrode and an Ag/AgCl as a reference electrode. To calculate the number of electrons was considered the sum of the final electric charge (Q, corrected for baseline charge) for successive electrolysis. The number of electrons transferred was calculated for each mole of **HQ** since the overall net charge, and using Faraday equation ($Q_{net} = n \times F\ e$, where n = number of moles, F = Faraday constant (96 500 C mol^{-1})

and e = number of electrons). The electrolysis was carried out by applying 100 mV more than the oxidation potential peak obtained by VPD (Table 1). Coulometric studies on the oxidation of each compound revealed an average of 1.9 ± 0.1 transferred electrons. Table 1 summarizes peak oxidation potentials and number of electrons obtained for different derivatives in an acetonitrile medium. Thus, an influence by substituent on the transferred electrons in the redox process was not observed.

3.4. Cyclic voltammetry characterization

The electrochemical behavior of **HQ** and **HQ** substituted was carefully investigated at a bare GCE in acetonitrile containing 0.1 M tetrabutylammonium perchlorate (TBAP) using cyclic voltammetry. These experiments were carried out at different sweep rates ranging from 0.01 to 1.5 V s^{-1}.

Fig. 4 shows the CV curves of 1.0 mM of **HQ2**. The separation between the anodic potential peak (E_{pa}) and the cathodic potential peak (E_{pc}) is, on the average, higher than 0.45 V for all the compounds studied. So, under these conditions, anodic signals were electrochemically irreversible as can be seen in Fig. 4A, and the peak current enhancements with increased scan rate for all compounds.[51]

Fig. 4B shows a linear relationship of i_p *vs.* the square root of the scan rate over the whole 0.001–1.5 V s^{-1} range, strongly suggesting that the redox reactions of **HQ** and **HQ** substituted are diffusion-controlled.[52] Plots of log i_p *vs.* log v had slopes close to 0.5 for both signals, confirming that currents were diffusion-controlled (Fig. 4C). The same analysis was carried out for all hydroquinones showing similar behaviors, a diffusion-controlled redox process. On the other hand, oxidation and reduction potential values were dependent on the sweep rates, supporting the electrochemically irreversible character of the processes of all compounds in this medium.[51] Fig. 5A confirms this phenomenon for **HQ3** because, in all cases, both anodic and cathodic processes (E_{pa}, E_{pc} and ΔE_p) show good

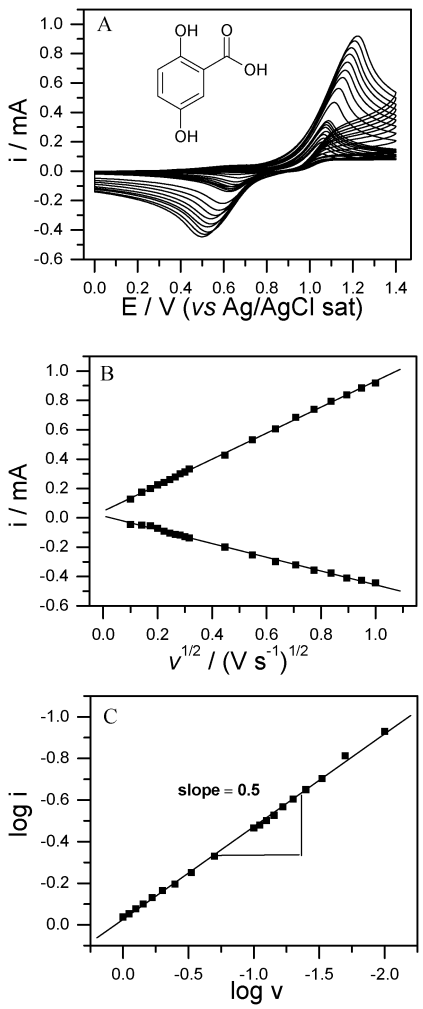

Fig. 4 (A) Cyclic voltammograms of 1.0 mM **HQ2** in acetonitrile + 0.1 M tetrabutylammonium perchlorate at different scan rates. (B) Linear relationship of i_p *vs.* $v^{1/2}$ of graph A. (C) log i *vs.* log v for the anodic process of A.

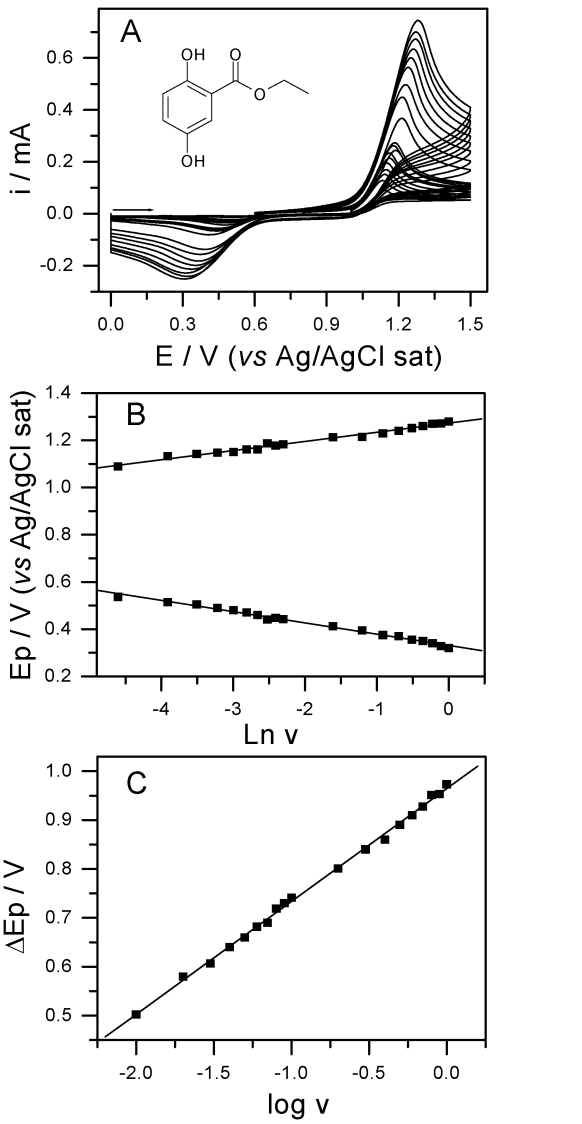

Fig. 5 (A) Cyclic voltammograms of 1 mM of **HQ3** in acetonitrile + 0.1 M tetrabutylammonium perchlorate at different scan rates. (B) Linear relationship between E_p and Ln v for A. (C) Linear relationship between ΔE_p and log v for A.

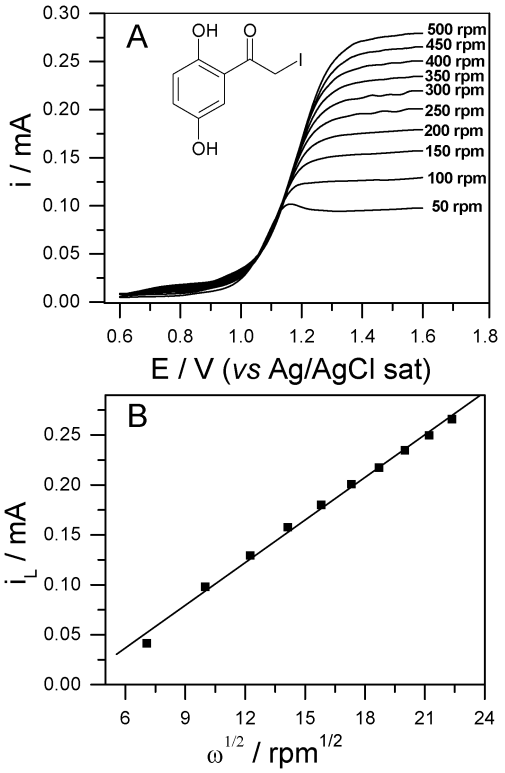

Fig. 6 (A) Typical hydrodynamic voltammetry on a glassy carbon rotating disk electrode of **HQ6** in acetonitrile + 0.1 M tetrabutylammonium perchlorate at different rotating rates. (B) Levich treatment of A.

linear relationships with ln v and log v, as can be seen in Fig. 5B and C, respectively.

3.5. Hydrodynamic voltammetry

Fig. 6 shows typical voltammograms on a graphite rotating disk electrode corresponding to 1.0 mM solutions of **HQ5**. This derivative, like the rest of the compounds, has one oxidation wave which did not show significant differences with the others. This supports the fact that the oxidation process involved a similar number of transferred electrons, and that it was also diffusion-controlled as mentioned before.

The relationship between the limiting currents and the square root of the rotation rate was linear for all compounds (Fig. 6), in agreement with Levich.[51] From these plots, the diffusion coefficients D were calculated (Table 1) and some differences were found between the derivatives, all of which showed lower D values than **HQ**: $D_{\mathbf{HQ}} = 3.42 \pm 0.05 \times 10^{-5}$ (cm^2 s^{-1}). A reasonable explanation of this decrease of the D values in **HQ** derivatives may be attributed to the active presence of substituents on the speed of diffusion to the surface electrode, influenced by a larger molecular volume. These results were confirmed by determination of geometrical parameters and condensed radical Fukui functions. The optimized geometrical parameters, HOMO energy, and condensed Fukui functions are summarized in Table 3. From the calculated results, it is found that a substituent in the aromatic ring increases the O1–H1 distance for **HQ1** to **HQ8**, compared to **HQ**. The differences between the O3···H1 distances and the O1–H1–O3 angles among the HQs are indicative of differences in the intramolecular hydrogen bond strength, as we mentioned above. These results suggest that the D value depends on both the nature and the position of the substituent on the aromatic ring, also confirming that bigger molecules have smaller diffusion coefficients.

The presence of bromine (**HQ4**) and iodine (**HQ5**) atoms in the *ortho*-position (Fig. 1) increases the molecular volume, decreasing the D value. No significant differences in D values were found when the substituent was a ketone (**HQ1**), a carboxylic acid (**HQ2**) or an ester (**HQ3**). In a decreasing order, coefficients obtained from the hydrodynamic experiments were $D_{\mathbf{HQ}} > D_{\mathbf{HQ7}} > D_{\mathbf{HQ2}} > D_{\mathbf{HQ3}} > D_{\mathbf{HQ1}} > D_{\mathbf{HQ8}} > D_{\mathbf{HQ4}} > D_{\mathbf{HQ5}} > D_{\mathbf{HQ6}}$. The determined D values show a similar tendency as reported by Valencia *et al.* for quinines and aromatic compounds in acetonitrile.[52]

4. Conclusions

Electrochemical oxidation of studied hydroquinone and hydroquinone derivatives in acetonitrile involves 2-protons and 2-electrons to give the quinone derivative as a final product. The electrochemical process is electrochemically irreversible with a ΔE_p higher than 0.45 V for all the compounds studied. The presence of substituents on the aromatic ring (carbonyl groups in the *ortho* position for example) shifted the redox potential to more anodic values respect to **HQ** because the presence of withdrawing groups decreases the electron density on the hydroxyl oxygen atom. A decrease in the D value with respect to hydroquinone was observed. Differences in the molecular structure of these hydroquinones significantly influence the characteristics of the C–O···H–O IHB present in them, affecting the electrochemical behavior. NBO calculations gave an insight into the electronic characteristics of the IHB and helped us to rationalize the relationship between the substituent on the aromatic ring, the presence of an IHB, and the oxidation potential of the hydroquinones studied in this work.

Acknowledgements

We are grateful to FONDECYT for grants 1130391, 3140286, 3120235 and 1140753, and DICYT USACH and ACT grant 1107.

References

1 R. H. Thomson, *Naturally occurring quinones*, Academic Press, London, New York, 1971.
2 J. Hirst, *Annu. Rev. Biochem.*, 2013, **82**, 551–575.
3 X. Q. Zhu, C. H. Wang, H. Liang and J. P. Cheng, *J. Org. Chem.*, 2007, **72**, 945–956.
4 J. R. Johnsson Wass, E. Ahlberg, I. Panas and D. J. Schiffrin, *J. Phys. Chem. A*, 2006, **110**, 2005–2020.
5 N. V. Rees, A. D. Clegg, O. V. Klymenko, B. A. Coles and R. G. Compton, *J. Phys. Chem. B*, 2004, **108**, 13047–13051.

6 M. Quan, D. Sanchez, M. F. Wasylkiw and D. K. Smith, *J. Am. Chem. Soc.*, 2007, **129**, 12847–12856.
7 C. C. Zeng and J. Y. Becker, *J. Org. Chem.*, 2004, **69**, 1053–1059.
8 P. H. Bernardo, C. L. Chai, G. A. Heath, P. J. Mahon, G. D. Smith, P. Waring and B. A. Wilkes, *J. Med. Chem.*, 2004, **47**, 4958–4963.
9 H. Ishikita, G. Morra and E. W. Knapp, *Biochemistry*, 2003, **42**, 3882–3892.
10 M. Wolf, A. Kappler, J. Jiang and R. U. Meckenstock, *Environ. Sci. Technol.*, 2009, **43**, 5679–5685.
11 E. J. O'Loughlin, *Environ. Sci. Technol.*, 2008, **42**, 6876–6882.
12 T. Dunlap, R. E. Chandrasena, Z. Wang, V. Sinha, Z. Wang and G. R. Thatcher, *Chem. Res. Toxicol.*, 2007, **20**, 1903–1912.
13 M. Chigr, H. Fillion, A. Rougny, M. Berlion, J. Riondel and H. Beriel, *Chem. Pharm. Bull.*, 1990, **38**, 688–691.
14 K. Haruna, H. Kanezaki, K. Tanabe, W. M. Dai and S. Nishimoto, *Bioorg. Med. Chem.*, 2006, **14**, 4427–4432.
15 E. J. Lana, F. Carazza and J. A. Takahashi, *J. Agric. Food Chem.*, 2006, **54**, 2053–2056.
16 C. H. Sun, Y. Wang, Z. Wang, J. Q. Zhou, W. Z. Jin, X. F. You, H. Gao, L. X. Zhao, S. Y. Si and X. Li, *J. Antibiot.*, 2007, **60**, 211–215.
17 L. Mendoza, R. Araya-Maturana, W. Cardona, T. Delgado-Castro, C. Garcia, C. Lagos and M. Cotoras, *J. Agric. Food Chem.*, 2005, **53**, 10080–10084.
18 I. Ali, F. G. Khan, K. A. Suri, B. D. Gupta, N. K. Satti, P. Dutt, F. Afrin, G. N. Qazi and I. A. Khan, *Ann. Clin. Microbiol. Antimicrob.*, 2010, **9**, 7.
19 S. K. Berezin and J. T. Davis, *J. Am. Chem. Soc.*, 2009, **131**, 2458–2459.
20 H. Mitsuda, M. Miyazaki, I. B. Nielsen, P. Çarçabal, C. Dedonder, C. Jouvet, S.-i. Ishiuchi and M. Fujii, *J. Phys. Chem. Lett.*, 2010, **1**, 1130–1133.
21 H. G. Upritchard, J. Yang, P. J. Bremer, I. L. Lamont and A. J. McQuillan, *Langmuir*, 2007, **23**, 7189–7195.
22 S. Patai and Z. Rappoport, *The Chemistry of the quinonoid compounds*, Wiley, Chichester, New York, 1988.
23 T. M. Alligrant, J. C. Hackett and J. C. Alvarez, *Electrochim. Acta*, 2010, **55**, 6507–6516.
24 P. D. Astudillo, J. Tiburcio and F. J. González, *J. Electroanal. Chem.*, 2007, **604**, 57–64.
25 T. F. Markle and J. M. Mayer, *Angew. Chem.*, 2008, **47**, 738–740.
26 J. Bonin, C. Costentin, C. Louault, M. Robert, M. Routier and J. M. Saveant, *Proc. Natl. Acad. Sci. U. S. A.*, 2010, **107**, 3367–3372.
27 T. J. Meyer, M. H. Huynh and H. H. Thorp, *Angew. Chem.*, 2007, **46**, 5284–5304.
28 T. F. Markle, I. J. Rhile, A. G. Dipasquale and J. M. Mayer, *Proc. Natl. Acad. Sci. U. S. A.*, 2008, **105**, 8185–8190.
29 M. Sjodin, R. Ghanem, T. Polivka, J. Pan, S. Styring, L. Sun, V. Sundstrom and L. Hammarstrom, *Phys. Chem. Chem. Phys.*, 2004, **6**, 4851–4858.
30 M. Sjodin, T. Irebo, J. E. Utas, J. Lind, G. Merenyi, B. Akermark and L. Hammarstrom, *J. Am. Chem. Soc.*, 2006, **128**, 13076–13083.
31 J. N. Schrauben, M. Cattaneo, T. C. Day, A. L. Tenderholt and J. M. Mayer, *J. Am. Chem. Soc.*, 2012, **134**, 16635–16645.
32 K. S. Feldman, D. K. Hester II and J. H. Golbeck, *Bioorg. Med. Chem. Lett.*, 2007, **17**, 4891–4894.
33 G. Armendáriz-Vidales, E. Martínez-González, H. J. Cuevas-Fernández, D. O. Fernández-Campos, R. C. Burgos-Castillo and C. Frontana, *Electrochim. Acta*, 2013, **110**, 628–633.
34 G. Zhao, M. Li, Z. Hu, H. Li and T. Cao, *J. Mol. Catal. A: Chem.*, 2006, **255**, 86–91.
35 H. Lund and O. Hammerich, *Organic electrochemistry*, M. Dekker, New York, 2001.
36 M. A. Bhat, *Electrochim. Acta*, 2012, **81**, 275–282.
37 T. A. Enache and A. M. Oliveira-Brett, *J. Electroanal. Chem.*, 2011, **655**, 9–16.
38 Y. Wang, S. R. Belding, E. I. Rogers and R. G. Compton, *J. Electroanal. Chem.*, 2011, **650**, 196–204.
39 Y. Zhang and J. B. Zheng, *Electrochim. Acta*, 2007, **52**, 7210–7216.
40 A. E. Reed, L. A. Curtiss and F. Weinhold, *Chem. Rev.*, 1988, **88**, 899–926.
41 A. Lammermann, I. Szatmari, F. Fulop and E. Kleinpeter, *J. Phys. Chem. A*, 2009, **113**, 6197–6205.
42 A. E. Shchavlev, A. N. Pankratov and V. Enchev, *J. Phys. Chem. A*, 2007, **111**, 7112–7123.
43 F. Weinhold, *Nature*, 2001, **411**, 539–541.
44 V. Pophristic and L. Goodman, *Nature*, 2001, **411**, 565–568.
45 P. R. Schreiner, *Angew. Chem.*, 2002, **41**, 3579–3581.
46 E. Lestini, K. Nikitin, H. Muller-Bunz and D. Fitzmaurice, *Chemistry*, 2008, **14**, 1095–1106.
47 L. C. King and G. K. Ostrum, *J. Org. Chem.*, 1964, **29**, 3459–3461.
48 J. A. Valderrama, C. Zamorano, M. F. Gonzalez, E. Prina and A. Fournet, *Bioorg. Med. Chem.*, 2005, **13**, 4153–4159.
49 M. J. Frisch, G. W. Trucks, H. B. Schlegel, G. E. Scuseria, M. A. Robb, J. R. Cheeseman, V. G. Zakrzewski, R. E. Stratmann, J. C. Burant and S. e. a. Dapprich, Wallingford, CT, 2004.
50 L. Goodman and R. R. Sauers, *J. Comput. Chem.*, 2007, **28**, 269–275.
51 R. G. Compton and C. E. Banks, *Understanding voltammetry*, World Scientific, Singapore, Hackensack, NJ, 2007.
52 D. P. Valencia and F. J. González, *Electrochem. Commun.*, 2011, **13**, 129–132.

